

Failure and Acoustic-Emission Response of Plasma-Sprayed ZrO_2 -8 wt% Y_2O_3 Coatings

N. R. SHANKAR, C. C. BERNDT, AND H. HERMAN

Dept. of Materials Science and Engineering, State University of New York
Stony Brook, NY 11794

It is critical to understand fundamental failure processes in order to design coatings for engineering purposes. The failure of ZrO_2 -8 wt% Y_2O_3 plasma-sprayed coatings is examined in the present work. The coatings were incorporated in a tensile-adhesion test arrangement and the acoustic emission (AE) was monitored. The AE generated during failure is related to the cracking process, and these are both related to the fracture morphology. Heat treatment of the coating affected changes in the AE count-rate distribution. This may be interpreted in terms of the morphological features of the coating. The relationship of the bond-strength tests to AE and fracture behavior give insight into the mechanism of adhesion of plasma-sprayed coatings.

I. Introduction

Plasma-sprayed ceramic coatings are used in a wide range of applications in which they are subjected to stresses which may be mechanical and/or thermal.¹ The durability of these coatings is in most cases limited by their adhesion strength to the substrate. The adhesion of these coatings is conventionally determined by the tensile-adhesion test (TAT)² in which a support bar is attached to the coating/substrate assembly by means of an organic epoxy having a tensile strength greater than that of the coating.

The TAT results exhibit a wide scatter³ which is due to the nature of the test and the coating microstructure. For example, preparation of the test specimen involves the use of an epoxy which cures at an elevated temperature, possibly resulting in penetration of the epoxy into the porous coating,⁴ misalignment between the coated substrate and the support bar,⁵ etc.⁶ Also, plasma-sprayed coatings have residual stresses, cracks, and porosity with the result that the structural and material characteristics can exhibit large variations from one specimen to another. Tensile-adhesion-test results generally show a large statistical spread and, in fact, TATs on other materials have been shown to follow a negatively skewed Kase distribution.¹

Tensile-adhesion-test failure modes are broadly classified into two types: cohesive, in which the failure occurs totally within the coating, and adhesive, in which the failure occurs at the interface between the coating and the substrate. Actually, both types of failure occur in the same specimen, and, therefore, the characterization of bond strength by a single number is far too simplistic. Such data do not contribute to an understanding of fundamental coating properties nor do they contribute to an understanding of failure mechanisms.

The present paper describes TATs which have been coupled with the technique of acoustic emission (AE).⁸ Acoustic emission, in the context of the present work, represents elastic waves arising from the generation and prop-

agation of cracks. Monitoring of AE, combined with postfailure examination of the fracture surfaces, will differentiate among various failure mechanisms.⁹ It will, in fact, be shown that cumulative AE counts up to failure correlate with the bond strength of the coatings.

A Y_2O_3 - ZrO_2 powder was examined in the present work. The probable condition-of the spray particles on arrival at the substrate was investigated by plasma spraying directly into H_2O (termed " H_2O quench"). The particle-size distribution, particle shape, and degree of melting were characterized for the powder in the as-received and H_2O -quenched conditions. These parameters are linked to the failure mode and the AE energy generated during a test. Heat treatment of the oxide coatings resulted in changes in bond strength, mode of fracture, and AE counts, as compared with the as-sprayed coatings.

Further work is currently being carried out to introduce precracks and to combine the techniques of AE and fracture mechanics to achieve a more fundamental understanding of coating adhesion and failure. This preliminary work points to the potential of using AE techniques to study coating failure and, hence, coating integrity. This understanding of fundamental coating-failure mechanisms and inherent material properties and structure is crucial for the engineering design and future development of protective ceramic coatings.

II. Experimental Procedure

Yttria-stabilized ZrO_2 (YSZ) powder, of chemistry and powder characteristics shown in Table I, was initially plasma sprayed into H_2O using plasma-spray parameters given in Table II. This was done with the view of characterizing the degree of melting and the effect of the plasma effluent on powder shape, size, and distribution.

Particle-size distribution for both the as-received and the H_2O -quenched powders was determined by sieving (7.5-cm-diameter sieves of woven Cu) for ≈ 8 h, so that there would be no subsequent change in the distribution on further sieving.

The oxide was also plasma sprayed with the same spray parameters as in Table II onto ends of cylindrical steel substrates conforming to specifications of the TAT.² As per accepted practice, prior to plasma spraying the substrate surface was prepared by grit blasting to achieve an "anchor pattern." A bond coat was not employed in these tests. In experiments currently underway, the effects of various bond-coat formulations are being taken into consideration. The average deposit thickness was 0.5 mm, and some coatings were also heat-treated for various times by encapsulating them in quartz tubes which had been back flushed (to 0.00133 Pa (0.00001 torr)) with Ar. A gas pressure of 20.3 kPa (0.2 atm) was maintained (at ambient temperature), resulting in a pressure of 101 kPa (1 atm) at the heat-treatment temperature of 1150°C. Following heat treatments of 1 or 10 h, the specimens were furnace cooled to room temperature.

The failure of the as-sprayed and heat-treated coatings were monitored by AE methodology in conjunction with a TAT. The experimental arrangement is shown in Fig. 1. Careful specimen preparation is essential, and attention is drawn to the following details with regard to the experimental techniques. The cylindrical substrate with the plasma-sprayed coating was attached to the support bar by an adhesive* and aligned in a jig. The entire assembly then was cured at 120°C for 40 min. Excess adhesive was removed from the cylinder side using emery paper with the specimen rotating on a lathe. The specimen

was then held by a self-aligning device on a tensometer,' ensuring uniaxial loading. The AE transducer was attached to the flat side of the support bar with a constant-force clamp and a couplant which increases acoustic sensitivity. Output from the transducer was preamplified and then amplified to a 100-dB gain. The amplified voltage was then compared with an automatic threshold voltage (which compensates for background and system noise), and each crossing of this threshold voltage was counted by the signal processor as a ringdown count. Also monitored was the root mean square (rms) amplified voltage, which is related to the intensity of the generated AE. The tests were carried out at a constant strain rate of 0.3 mm/min^{-1} , and the load to fracture was determined. The load-extension curve was not measured during a test since the engagement of the recording device gave rise to spurious acoustic phenomena which masked the AE activity arising from any cracking process. However, it is common experience that TAT specimens exhibit a linear load-extension curve up to their failure load, at least when overall extension is measured. The possibility of gross localized strain inhomogeneities occurring during a TAT is the subject of another investigation currently being carried out. Measurements were made of both the AE count rate and the corresponding rms voltage of the signal during the bond test. As will be shown later, the cumulative number of counts can be determined from the count-rate data.

The as-sprayed surface and the fracture surfaces from both the adhesive- and cohesive-fracture regions of the oxide coatings were examined by scanning electron microscopy (SEM). It should be noted that all fracture surfaces are viewed from the perspective of the substrate (thus, the relative position of the substrate is "on top of the page" and the coating is "facing up").

III. Results

Particle Characteristics

The YSZ particles, both as-received and H_2O -quenched, are shown in Fig. 2. The particle-size distribution determined by sieve analysis is shown in Fig. 3. The porous structure of the powder is due to the production method in which micrometer-size ZrO_2 and Y_2O_3 are mixed together and reacted at a high temperature. Therefore, the effective surface area of the particle is greatly increased and this would increase the heat transfer to the particles during the plasma-spraying process.

Water-quenching of the plasma-melted YSZ yields a large number of unmelted particles (Fig. 2(C)). Figure 2(D) shows a partially melted particle in which the surface was more molten than the core. The particles also exhibit many microcracks, which are expected to play an important role in any failure process. Water-quenching only influenced the particle-size distribution by slightly decreasing the range of particle diameters from $\approx 50 \mu\text{m}$ to $40 \mu\text{m}$ (Fig. 3).

Coating Characterization

Examination of the coating surface can give insight into the structure of the bulk of the coating. As shown in Fig. 4, the YSZ coating has many fine cracks (region "a"), as well as unmelted particles of irregular shape (region "b"). A most significant feature is, therefore, that unmelted (or partially melted) YSZ particles confirm a relatively rough surface to the coatings, compared with the fully molten case, and this is an excellent "key" to overlaying molten

particles. Thus, the overall view is that the bulk of the coating consists of many fine features which derive both from partial melting of the particles and from significant microcracking. This kind of defect structure should be clearly distinguished from a structure in which the particles are fully melted, since in this case the defects would essentially be planar and oriented parallel to the substrate surface.

AE Monitoring during TAT

Acoustic emission was monitored during the TAT from the initiation of load application until fracture. The ringdown count rate and rms voltage were measured during the tests. The two types of AE spectra that were observed are shown in Fig. 5 and described below.

- 1) The count rate increased gradually to an approximately constant value prior to increasing at failure—i.e., the curves are skewed left (Fig. 5(A)(i)).
- 2) The count rate increased initially, followed by a decrease to a lower level prior to increasing at failure—i.e., the curves are skewed right (Fig. 5(B)(i)).

The above nomenclature will be retained when discussing the statistical analysis of the results.

A TAT specimen without a coating gave insignificant AE counts. Therefore, all the AE phenomena are considered to result from processes associated with the coating.

The rms voltage vs time curves exhibited corresponding features with respect to their skewness. However, the overall rms-voltage behavior was slightly more complex with regard to the relative stability. Therefore, it is expected that the fluctuation in the rms-voltage signal arises from the various cracking processes during failure of the coating. In all tests, the rms voltage and count rate increased significantly during final failure of the coating.

The cumulative counts were obtained by integrating the count-rate data shown in Fig. 6. The relationship of the integrated AE counts with bond strength is shown in Fig. 7. These results are summarized in Table III. A statistical analysis of the count-rate data will be given in the Discussion.

Figure 6 shows results for YSZ coatings which have been as-sprayed and in some cases treated according to the conditions indicated as in the figure. The high slopes immediately prior to failure are due to the high counts generated at fracture. The specimens are numbered according to their bond strengths, with 1 having the highest bond strength and 6 the lowest bond strength among the as-sprayed coatings. Similarly, "a" has the highest bond strength and "c" the lowest bond strength among the heat-treated coatings. There was a 100-h delay between spraying and grit blasting for specimen "d." Both heat treatment and delay after grit blasting decrease bond strength and the corresponding cumulative AE counts. Decreases in AE counts and in bond strength are dependent on the length of heat treatment, with 10-h treatments being more detrimental than the 1-h treatment. Specimen 6 seems to be an exception in that it generated high AE counts but had a low bond-strength value. It should be pointed out that this is due, in part, to a rapid increase in acoustic activity during the first 9 s of the test, which is shown graphically as a high initial slope. The same phenomenon can be observed for specimen 1 in which there is a distinct knee in the AE count vs time curve after 10 s. These two specimens were unique in exhibiting this behavior, as were their rms volt-

age-vs-time curves which followed behavior of Fig. 5(B)(i). The sudden rise in the AE count rate (Fig. 5(B)(ii)) and the different nature of these spectra compared with that of the other coatings (Fig. 5(A), (i) and (ii)) are due to a different fracture mechanism occurring in these two coatings.

The total AE counts are plotted against the bond strength in Fig. 7. The general trend observed is that a high bond strength gives rise to a high acoustic-emission count, the relationship following a power law. The as-sprayed YSZ specimens have much greater bond strengths than do the thermally treated YSZ coatings. The implications of these results in terms of fracture mechanisms will be discussed later.

Fracture Surfaces

Fracture surfaces were examined using SEM to characterize the fracture surfaces. The YSZ coating exhibited regions of both cohesive and adhesive failure. Neither pure adhesive nor pure cohesive failures were observed over any given fracture surface and are, in fact, rarely observed for any TAT. A description of a fracture mode will imply that the exact force-mode relationship is known. In the present tests, the deforming force is tensile; however, the complex microstructure of the coatings results in shear deformation as well. These complexities will be considered when the fracture mechanisms are discussed.

The adhesive-fracture region of the YSZ coating is shown in Fig. 8(A). Many cracks are apparent, and the fracture appears interlamellar, as noted by the distinct flat shapes of several of the particles. However, it should also be noted that the adhesive-failure morphology may have the characteristic of exhibiting very fine features since failure in this case would occur quite close to the substrate through the highly deformed and broken-up particles of the initially deposited material. These regions are more clearly distinguished at regions closer to the substrate part of the TAT specimen. Cohesive failure also exhibited flattened areas characteristic of interlamellar failure as shown in region "a" of Figure 8(B). There were also areas in which lamellar failure was observed in profile (i.e. the lamellae are viewed edge-on in area "a" of Fig. 8(B)): the resultant failure morphology is terraced or stepped. The fracture surface, therefore, shows more depth than the case of adhesive failures which are, in turn, relatively flat and planar.

IV. Discussion

The relationship between bond strength and AE is emphasized in the present study. Since both the coating integrity and noise-generating cracking processes are connected, it would seem worthwhile to develop an understanding of failure modes as manifested by AE. As such, the following will be emphasized:

- 1) The relationship of the **H₂O-quenched** powders to the sprayed deposit;
- 2) Statistical analysis of the AE data and its relevance;
- 3) Fracture mechanisms of the coatings and the correlation to initial powder morphology and the microstructure; and
- 4) Implications of the test results in regard to coating performance.

Water Quenching of Powders

A major problem which is always encountered when examining the structures of plasma-sprayed coatings is in ascertaining the prior history of the

particles. Thus, the particles were quenched immediately prior to impact against the substrate so that their shape and degree of melting could be studied. There are arguments against this treatment **especially** for a rigorous examination of the particle-size distribution and the individual particle chemistry. For example, it is impossible to carry out an exact sizing analysis because some powder is inevitably lost during the plasma-spraying operation, and this is most apparent for the smaller particles. **Also**, conditions during quenching **may not be** identical to conditions encountered **by** the particles during coating formation.

The YSZ powder did not exhibit any significant **particle-distribution** change after quenching in H_2O and, therefore, the micrographs (Figs. 2(C) and 2(D)) are a good representation of the particle morphology immediately prior to **splat** deformation. Areas are exhibited which show partial melting of particles, internal porosity, and microcracks on the surface. Microcracks and porosity arise due to the **H_2O -quenching** operation but are also present in plasma-sprayed coatings (Fig. 4). The main feature is that many particles are not completely melted by the plasma effluent, and this is an excellent surface to permit **the** mechanical anchoring of other overlaying, semimolten particles.

Statistical Analysis

As indicated in Fig. 7, coatings which exhibit a high bond strength also exhibit a high AE count. It would, therefore, be interesting to attempt to relate high count-rate acoustic emissions with the various types of samples, their bond strengths, and fracture morphologies. The AE features of particular interest are the most frequent count rates and the period during a test in which high and low count rates occur (**i.e.** the progressive count-rate sequence). The AE data on final failure of the specimen are not included in this analysis.

As-Sprayed YSZ

The as-sprayed YSZ coatings exhibited the most complex AE response. The two types of count-rate distributions that were observed have already been described (**i.e.** skewed left or right as in Fig. 5); however, trends during the test were most easily observed by plotting the histogram of frequency vs count rate. The results of two tests which represent the above behavior are shown in Fig. 9, in which the numbers refer to the sequence (in seconds) of acoustic events. It is clear that both distributions have a high frequency at a particular count rate; therefore, these curves have been treated by comparing them with normal distributions. The features of the histograms are:

- 1) Skewed left (Fig. **5(A)(ii)** and Fig. **9(A)**)—**the** count rate increases with time. Prior to failure, the count rate is maximum.
- 2) Skewed right (Fig. **5(B)(ii)** and Fig. **9(B)**)—**the** distribution is bimodal. Initially, the count rate is high, but after about one-third of the test time the count rate decreases significantly with a minimum occurring just prior to failure.

Even though the AE response of the various tests can be classified, as above, it is still difficult to reconcile the magnitude of the AE cumulative counts and the count rate (both with respect to time) to the tensile-adhesion strength. Table **IV(A)** shows the results of the statistical analysis for the **as-sprayed** YSZ coatings. There are a number of complicating factors which make it difficult to detect any trends. For example, some samples (Nos. 2 and 3) fail in the mixed **adhesive/cohesive** mode, and other samples (Nos. 1 and

6) exhibit a bimodal count-rate distribution. By noting how different **groups of data** affect the magnitude of the coefficient of variance, the data have **been treated** so that atypical acoustic counts have been discounted. The trends from the analysis of moments (*i.e.* the mean, standard deviation, skewness coefficient, and kurtosis coefficient¹⁰) are:

- 1) A bimodal distribution leads to the highest total **acoustic-emission** count (specimens 1 and 6) and also gives rise to a knee in the cumulative AE curve.
- 2) The specimen which exhibited the lowest bond strength (No. 6) also showed the most normal skewness and kurtosis parameters. Thus, even though the mean count rate was high, it appears as if the cracks were pre-existing prior to the test, since there was no dramatic increase in the count rate.
- 3) Samples which failed in a mixed mode (Nos. 2 and 3) had a high mean count rate as well as left skewness and a high kurtosis.
- 4) Samples with low mean counts (Nos. 4 and 5) also had a high standard deviation and coefficient of variance. This may mean that the phenomena giving rise to the AE are steady-state and that cracking occurs continuously on a small scale.

The main features of the as-sprayed YSZ coatings will be compared for the other coatings (Table IV(B)).

Treated YSZ

The count rate vs time curves for the treated YSZ coatings were all skewed left and exhibited an increase in count rate with the duration of the test. All of the tests exhibited a high count rate during the final stages, this feature being indicated in Table IV(B) by a difference in the mean count rates for different data sets. The overall mean levels are similar to those for adhesive failure of the as-sprayed YSZ coatings (*e.g.*, specimens 4 and 5; specimens 1 and 6 have been discounted because they are bimodal). A summary of the analysis is given in Table V.

Fracture Mechanisms

The count-rate distribution must be correlated to microstructure and bond strength for a detailed analysis of coating-failure mechanisms (Table VI). Other **workers**^{11,12} have used AE methods to characterize the bond strength of organic adhesives which were tested by the lap-shear technique. An interesting **result**¹¹ was that faulty preparation of joints, which resulted in low bond strengths, could also be detected by greater amounts of emission at relatively low loads. This is clearly analogous to the case of specimen 6 in the present work, and, thus, the very high count rate observed during the initial 9 s of the test may represent a different cracking mechanism. Further analysis of the AE phenomena would entail a study of waveform and **spectra**.¹³ A simple, qualitative approach is, however, considered in the following discussion. The magnitude of the count rate is proportional to the number of cracks or the growth of cracks, so that a large count rate represents either the nucleation of new cracks or the growth and interactions among existing cracks. Therefore, the processes for the monomodal distributions which showed increasing count rate are crack formation and growth.

Generally, the mean count rate was noted to increase with the bond strength, inferring that more extensive crack interactions occurred for the coatings. The

cracking phenomena in the most simple cases are either separation at the substrate interface (adhesive) or between lamellae (cohesive); however, cracks are still generated over the bulk of the coatings. **Cracking of the YSZ coatings** is quite complex due to the fact that only portions of many particles actually melted during spraying (Fig. 4). The unmelted regions act as anchoring points for overlaying lamellae, and these fine features of the microstructure must be broken during failure testing. Thus, the total number of nucleating points for cracks is considerably greater than the mean lamellar size. Additionally, the coatings also exhibit a minor component of cohesive failure where failure occurred across lamellae in a shear fashion. **Supplementary** information to verify this mechanism is gained from the fracture morphology of the YSZ coatings which show very fine features.

The above observations lead to an understanding of the failure processes which result in a bimodal distribution of the YSZ coatings. The minimum-size crack will be limited to the smallest microstructural feature, i.e. the approximately micrometer-size features of the particles. The defect network initially consists of cracks of this fine nature, and these interact to form larger cracks. Thus, the count rate decreases during an experiment. Eventually, the cracking process occurs on a scale of events comparable to the particle size, and a second characteristic count rate begins to predominate. Both of these cracking modes contribute to the overall count rate, and their relative contributions toward the total number of counts are different.

The above analysis is further complicated on considering the transmission of AE energy through a highly defected material. A high number of cracks may establish a barrier to the AE waves and, thus, decrease the transmitted and, therefore, detectable count rate, this occurring more readily for large cracking between lamellae. In fact, a large variation of acoustic-emission response can be gaged from the wide fluctuation in the rms voltage (Figs. 5(A)(i) and 5(B)(i)), this being particularly significant for the YSZ coatings which failed in a bimodal fashion.

Heat treatment of the coating changes the microstructure. For the YSZ coatings containing numerous unmelted particles, the defects have a more planar distribution. Therefore, cracks follow a less tortuous path, and the adhesion strength, as well as the mean count rate, is low. The effect of heat treatment described above is, in fact, too simple due to other complicating factors, such as changes in residual strain distribution, phase, and composition. There are, however, no data currently available on these matters.

A delay in spraying after grit blasting decreases the adhesion strength and mean count rate. This is undoubtedly due to processes at the substrate surface such as oxidation.

A significant feature of AE tests is that a high acoustic count can be related to a greater mean crack path and that this behavior can be related to either a mixed-mode failure and/or a fracture morphology which exhibits very fine features. The interpretation of the AE count rate is more complex. The overall trend is that coatings with a high count rate also exhibit the highest strength; however, relaxation of residual stresses in the coating, together with transmission of acoustic energy through a deformed structure, complicates this analysis.

Implications and Closing Comments

It is important to note the relevance of the tests carried out in the present

work to the specific application which coatings experience during service life. For example, it is reasonable to question how room-temperature tensile-adhesion tests can be related to coatings which fail at service temperatures $>1100^{\circ}\text{C}$. The analysis makes no claim that bond-strength data can be extrapolated to high temperature, corrosive environments, but it is considered that there is a correlation with regard to the mechanisms of failure. No single feature of the plasma-spraying process controls the fundamental adhesion property of coatings; the particle characteristics, plasma-spray variables, and subsequent operating environment all interact to determine specific coating properties. However, the failure mechanism can be closely followed by the technique of acoustic emission, and it is possible to distinguish different failure phenomena from the AE count and count-rate spectra. This is a powerful tool to aid in the understanding of the fundamental properties of plasma-sprayed coatings.

V. Conclusions

This work has examined the failure properties and bond strengths of a YSZ coating produced by plasma spraying. The coatings were tested in the standard manner,² both in the as-sprayed condition and after heat treatment (for 1 and 10 h at 1150°C) and, in one case, after a 100-h delay between grit blasting and spraying.

The bond strength of the YSZ coatings significantly decreased after heat treatment. The acoustic-emission count and count rates were statistically analyzed to assess trends in their behavior during the progress of a test. The average mean count rate was related to fracture processes which occur within the coating, and these correlated to the fracture-surface morphology. The partially molten nature of the YSZ particles provided sites for the mechanical anchoring of overlaying particles; thus, deformation occurred through the bulk of the coating. On the other hand, when the coating was treated the deformation zone was restricted to a planar area, and the strength of the coating decreased.

In the final analysis, before coatings can be designed for specific applications it is necessary that their failure-related engineering properties be ascertained. The present work has been aimed at understanding several fundamental aspects of the failure characteristics of these coatings.

References

- ¹(a) Stephan Stecura, "Two-Layer Thermal-Barrier Systems for Ni-Al-Mo Alloy and Effects of Alloy Thermal Expansion on System Life," *Am. Ceram. Soc. Bull.*, **61** [2] 256-62 (1982).
- (b) P. A. Siemers and W. B. Hillig, "Thermal-Barrier-Coated Turbine Blade Study," NASA Tech. Rept. No. CR-165351 on NASA Contract No. NAS3-21727, August 1981.
- (c) R. J. Bratton, S. K. Lau, and S. Y. Lee, "Evaluation of Present Thermal Barrier Coatings for Potential Service in Electric Utility Gas Turbines," NASA Tech. Rept. No. CR-165545 on NASA Contract No. NAS3-21377, July 1982.
- ²Standard Method of Test for Adhesion or Cohesive Strength of Flame-Sprayed Coatings," ASTM Designation C 633. 1982 Annual Book of ASTM Standards, Part 17, pp. 636-42. American Society for Testing and Materials, Philadelphia, PA.
- ³(a) F. J. Hermanek, "Determining the Adhesive Cohesive Strength of Thin Thermally Sprayed Deposits," *Weld. J.* (Miami), **57** [11] 31-5 (1978).
- (b) R. L. Apps, "The Influence of Surface Preparation on the Bond Strength of Flame-Sprayed Aluminum Coatings on Mild Steel," *J. Vac. Sci. Technol.*, **11** [4] 741-6 (1974).
- ⁴J. A. Catherall and K. E. Kortegas, "Measurement of Bond Strength of Flame-Sprayed Deposits," *Met. Const. Br. Weld. J.*, **4** [1] 11-3 (1972).
- ⁵W. E. Stanton, "The Mechanical Properties of Sprayed Metals for Engineering"; pp. 157-64, 312-4 in Proceedings of the Seventh International Metal Spraying Conference, Vol. I. Welding Institute, Abingdon, Cambridge, England, 1974.
- ⁶C. C. Berndt and R. McPherson, "Fracture Mechanics Approach to the Adhesion of Flame and Plasma Sprayed Coatings," *Trans. Inst. Eng. Aust.*, **ME6** [1] 53-8 (1981).

¹P. Kurzman and D. A. Klemme. "Discussion of Bond Strength Test Results in Terms of Mathematical Statistics," *J. Adhes.*, 7 [3] 203-13 (1975).

²W. Swindlehurst, "Acoustic Emission—1: Introduction," *Non-Destr. Test. (Guildford, Eng.)*, 6 [3] 152-8 (1973).

³N. R. Shankar, C. C. Berndt, H. Herman, and S. Rangaswamy, "Acoustic Emission from Thermally-Cycled Plasma-Sprayed Oxides": submitted for publication to the American Ceramic Society.

⁴(a) R. P. Runyon and A. Haber. *Fundamentals of Behavioral Statistics*, 2d ed.; Chapters 3, 5, 6, and 7. Addison-Wesley, Reading, MA, 1975.

(b) R. F. Sokal and F. J. Rohlf, *Biometry*, 2d ed.; Chapters 4 and 6. W. H. Freeman & Co., San Francisco, 1981.

⁵R. Hill, "The Use of Acoustic Emission for Characterizing Adhesive Joint Failure," *NDT Int.*, 10 [2] 63-72 (1977).

⁶G. J. Curtis, "Acoustic Emission Energy Relates to Bond Strength," *Non-Destr. Test. (Guildford, Eng.)*, 8 [5] 249-57 (1975).

⁷(a) D. E. W. Stone and P. F. Dingwall, "Acoustic Emission Parameters and Their Interpretation," *NDE Int.*, 10 [2] 51-62 (1977).

(b) R. Hill and R. W. B. Stephens, "Simple Theory of Acoustic Emission—A Consideration of Measurement Parameters," *Acustica*, 31 [4] 224-30 (1974).

⁸R. W. B. Stephens and A. A. Pollock, "Waveforms and Frequency Spectra of Acoustic Emissions," *J. Acoust. Soc. Am.*, 50 [3] 904-10 (1971).

*CONAP AD-3, Conap, Inc., Olean, NY.

¹Hounsfield Tensometer, Tensometer, Ltd., Croyden, England.

²AETC 204A, Acoustic Emission Technology Corp., Sacramento, CA.

Table I. Powder Characteristics.

Composition (wt%)	92ZrO ₂ 8Y ₂ O ₃
Production method	Prereacted
Powder size (μm)	
As-received	– 90+40
Water quenched	– 80+40

Table II. Plasma-Spray Parameters.

Arc voltage (V)	65
Arc current (A)	500
Plasma gas (m ³ ·h ⁻¹)	
Ar (primary)	2.5-3.1
H (secondary)	0.4-0.7
Powder feed gas (m ³ ·h ⁻¹)	
Argon	1.1
Gas pressure (MPa)	
Ar	0.70
H	0.35
Powder feed rate (kg·h ⁻¹)	2.0-2.5
Spray distance (cm)	6-8

Table III. Acoustic-Emission Data for **YSZ** Plasma-Sprayed Coatings Subjected to Tensile-Adhesion Tests.

Specimen*	Failure stress (MPa)	Total AE counts [†]	Counts at failure	Mean rms voltage	Variation in rms voltage [‡]		Failure rms voltage
					Low	High	
1	39.8	99 440	8400	1.80	1.74	1.98	2.35
2	36.3	57 700	7120	1.97	1.97	2.07	2.40
3	34.1	40 600	4340	1.98	1.95	2.00	2.45
4	34.1	29 240	8800	1.65	1.65	1.83	2.50
5	32.0	26 100	12 140	1.60	1.58	1.63	2.50
6	30.5	54 540	8000	1.65	1.63	1.81	2.38
a	18.0	6400	2260	1.55	1.53	1.55	2.45
b	12.3	7460	3060	1.55	1.55	1.62	2.55
c	3.4	1000	820	1.52	1.50	1.55	2.33
d	17.8	11 250	2760	1.60	1.60	1.65	2.42

*Specimens 2 and 3 exhibited the mixed-mode **adhesive/cohesive** failures, whereas all the rest exhibited the predominantly adhesive mode.

[†]Failure counts have been included.

The "high" rms voltage was small when the mean rms voltage was close to the "low" value (**i.e.**, a small range of values).

^{||}**Data** from specimen "c" has not been included in the statistical analysis because there were only 3 data points.

Table IV. Statistical Analysis of AE Data of YSZ Coatings.*

Sample	Mean AE count rate	Standard deviation	Coefficient of variance	Skewness (gm/l)	Kurtosis (gm ²)	Data sets [†]
A. As-sprayed						
1	2529	694	27	0.45	3.61	36 all
	3011	886	29	-0.94	3.75	1-13
	{ 3406	425	12 [‡]	1.85	5.24	3-11, 13
	{ 2257	324	14 [‡]	0.26	2.60	14-36
2	1445	385	27	-0.87	4.72	1-35
3	1066	258	24	-1.88	7.30	1-34
4	619	265	43	1.36	8.34	1-33
5	465	154	33	-0.73	3.76	1-30
6	1662	594	36	0.16	3.63	1-28
	2044	902	44	-1.14	2.92	1-9
	{ 2613	174	7 [‡]	0.01	1.93	4-9
	{ 1481	180	12 [‡]	0.19	2.54	10-28
B. Treated						
a	460	268	58	0.83	2.41	1-9
	331	125	38 [‡]	0.10	1.38	1-7
b	403	216	54	0.94	2.83	1-11
	312	105	34 [‡]	-0.24	1.69	1-8, 10
d	530	410	77	0.50	1.71	1-16
	{ 196	96	49 [‡]	0.60	2.06	1-10
	{ 1005	195	19 [‡]	-0.19	1.66	11-16

*All measurements refer to the AE count rate.

[†]The data points which have been included in the particular analysis are indicated.

[‡]The best set of data points as judged by the coefficient of variance. This can be either monomodal or bimodal.

^{||}It is difficult to distinguish whether sample "d" is monomodal or bimodal; it has been considered to be monomodal.

Table V. Summary of Statistical Analysis of AE Data and Features of the AE Count-Rate Distributions.

Coating description	Count rate vs time distribution	Frequency vs count-rate distribution	Count-rate sequence
As-sprayed	Left skewness	Monomodal	Increases until failure
YSZ	Right skewness	Bimodal	Failure at maximum
		(1)	{ High mode first Count rate decreases
		(2)	{ Low mode second Count rate decreases Failure at minimum
Treated YSZ	Left skewness	Monomodal	Increases until failure Failure at maximum

Table VI. Relationship of AE Count-Rate Distribution to Bond Strength of YSZ Coatings.

Coating description	Distribution description	Mean AE count rate	Number of samples	Bond strength (MPa)
Monomodal				
As-sprayed	Count rate increases	1200	2	36.3, 34.1
		500	2	34.1, 32.0
Treated		420	4	18.0, 12.3, 3.4, 17.8
Bimodal				
As-sprayed	High count rate first Low count rate	3400–2600 2250–1480	2	39.8, 30.5

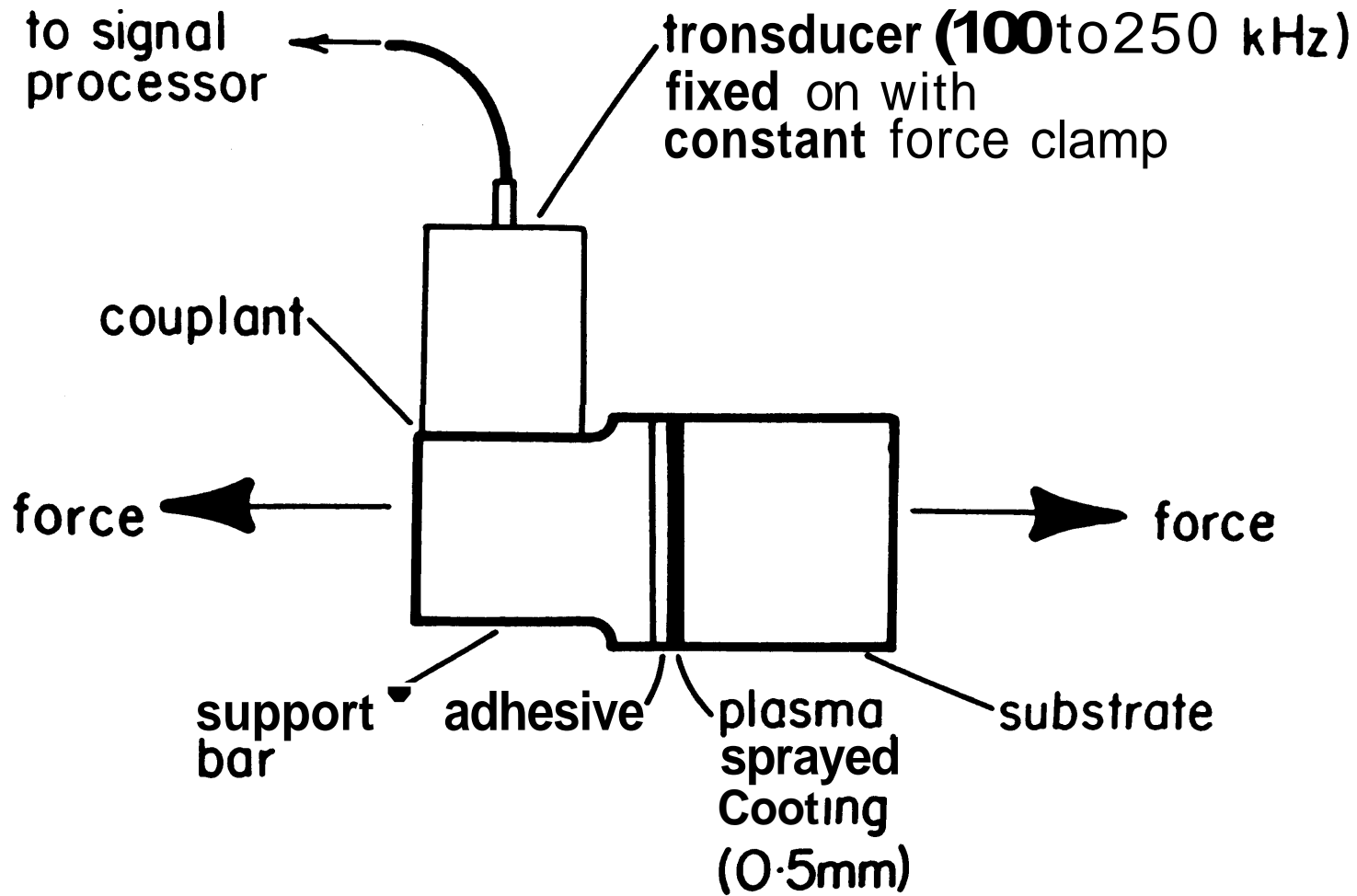
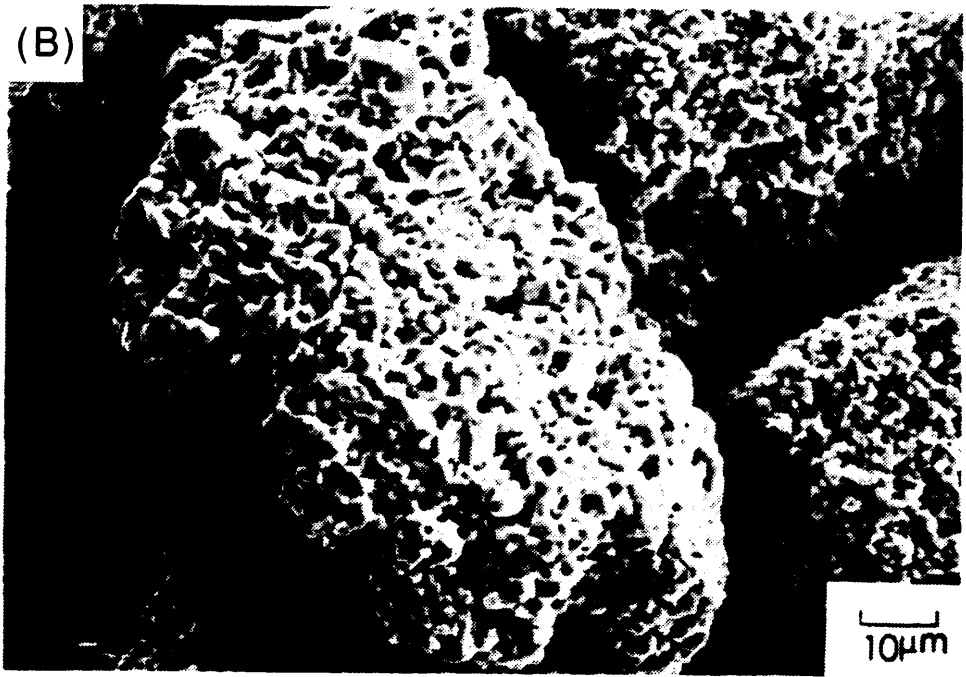
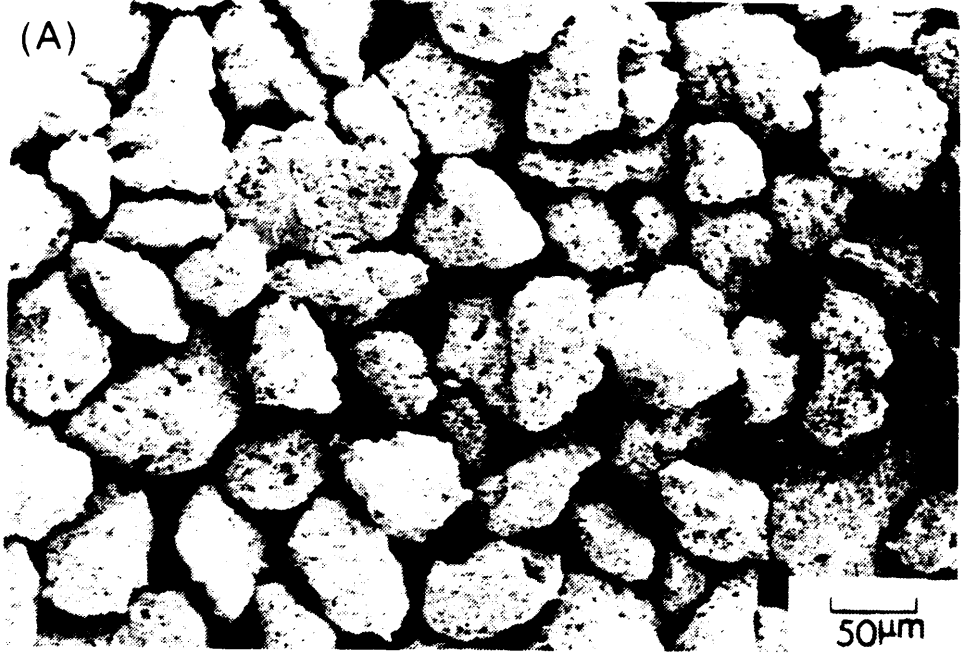


Fig. 1. Schematic of the experimental arrangement for acoustic-emission monitoring during the tensile-adhesion test.



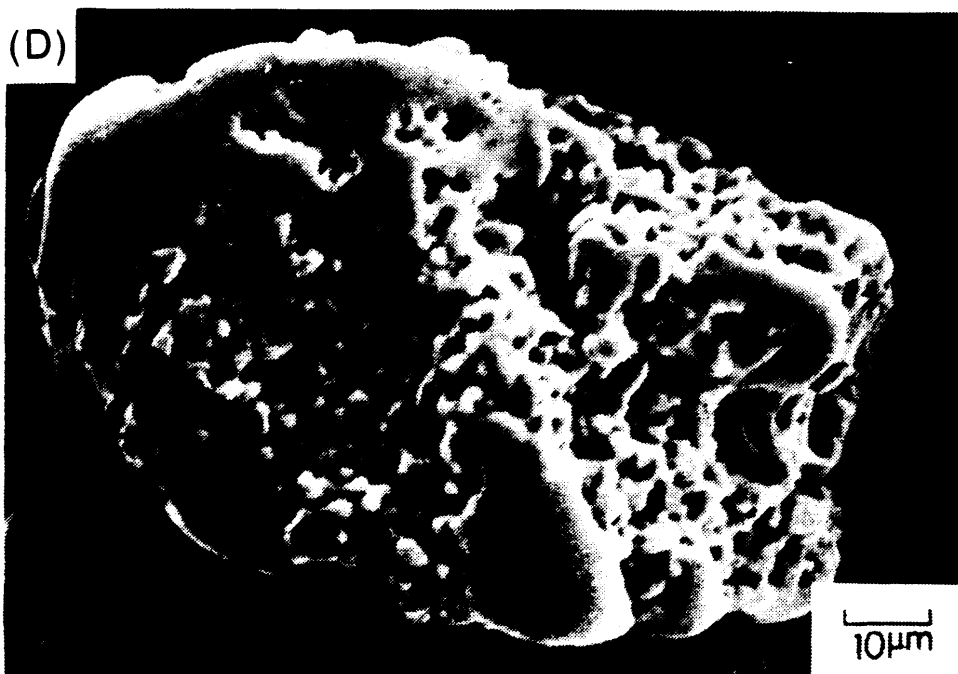


Fig. 2. Morphology of the YSZ powder: (A) as-received prereacted powder exhibiting irregular shape; (B) a single particle showing very fine surface features of 1 μ m in size; (C) H_2O -quenched YSZ powder showing considerable unmelting particles; and (D) a particle showing a partially melted surface and microcracks.

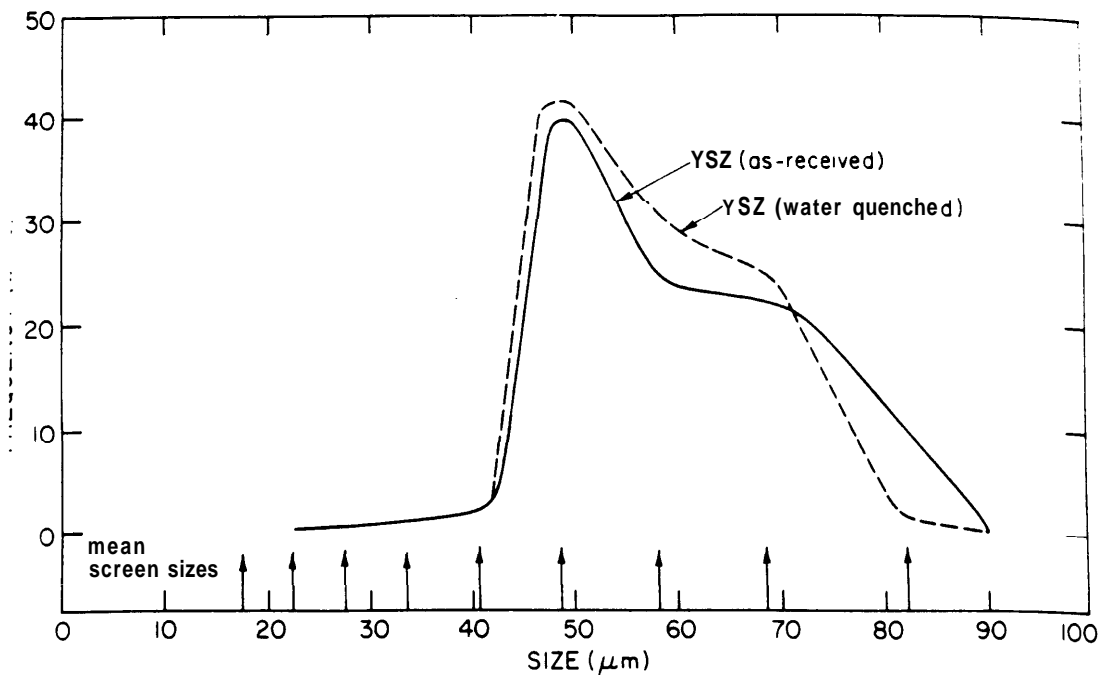


Fig. 3. Particle-size distribution of the as-received and H₂O-quenched YSZ powders.



Fig. 4. Surface of plasma-sprayed YSZ coating showing regions of fine cracks (region "a") and unmelted particles (region "b").

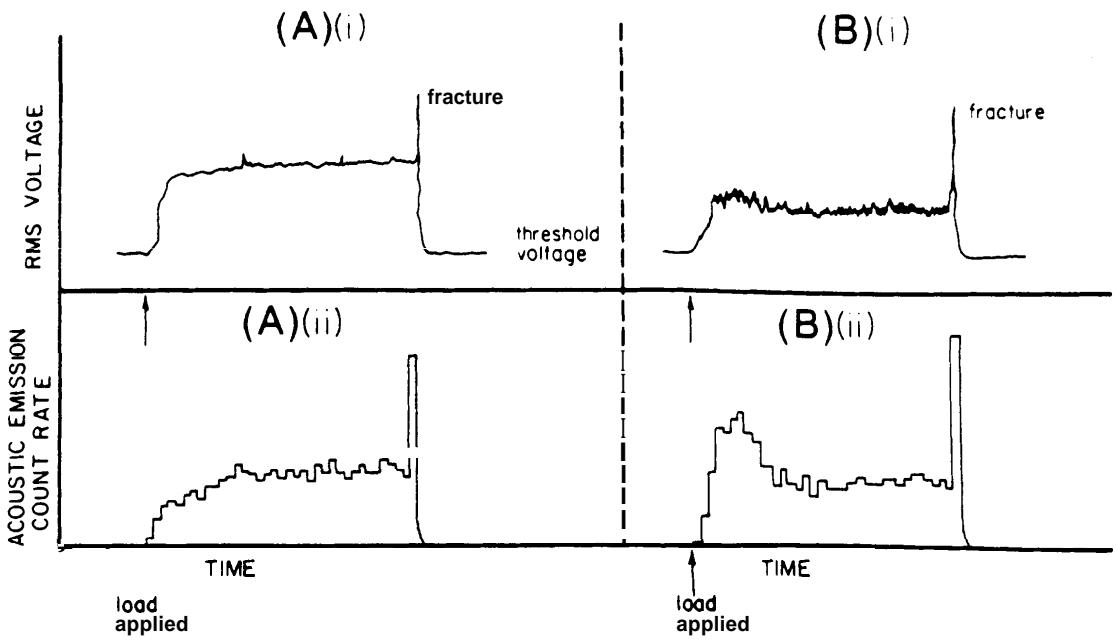


Fig. 5. Two types of AE spectra observed during the tensile adhesion test: (A(i)) the AE rms voltage increases gradually to an approximately constant value prior to increasing at fracture; (A(ii)) the corresponding AE count rate vs time curve; (B(i)) the AE rms voltage increases initially and then decreases to a lower value prior to increasing at fracture (also the **RMS** voltage is more unstable than in curve (A(i))); and (B(ii)) the AE count rate which corresponds to curve (B(i)).

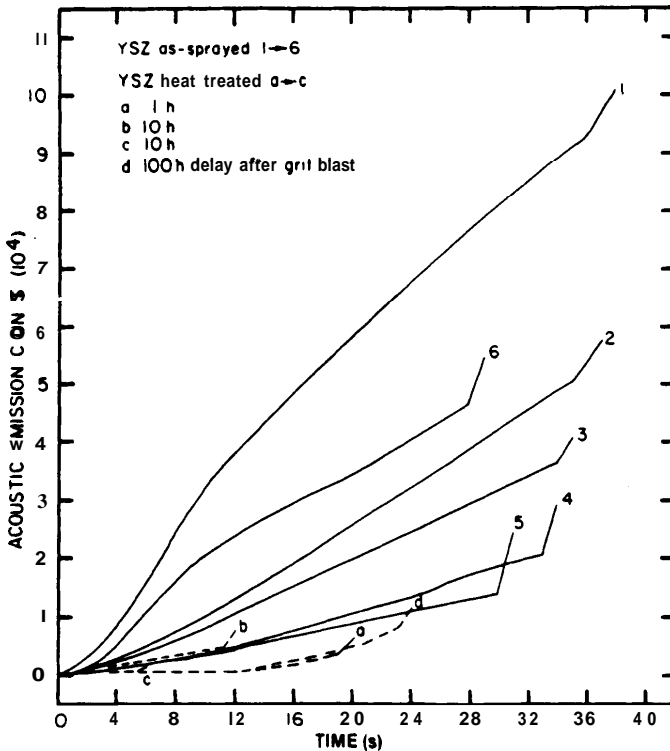


Fig. 6. Cumulative AE counts vs time of tensile-adhesion test for the as-sprayed **YSZ** coatings and coatings treated according to conditions as indicated.

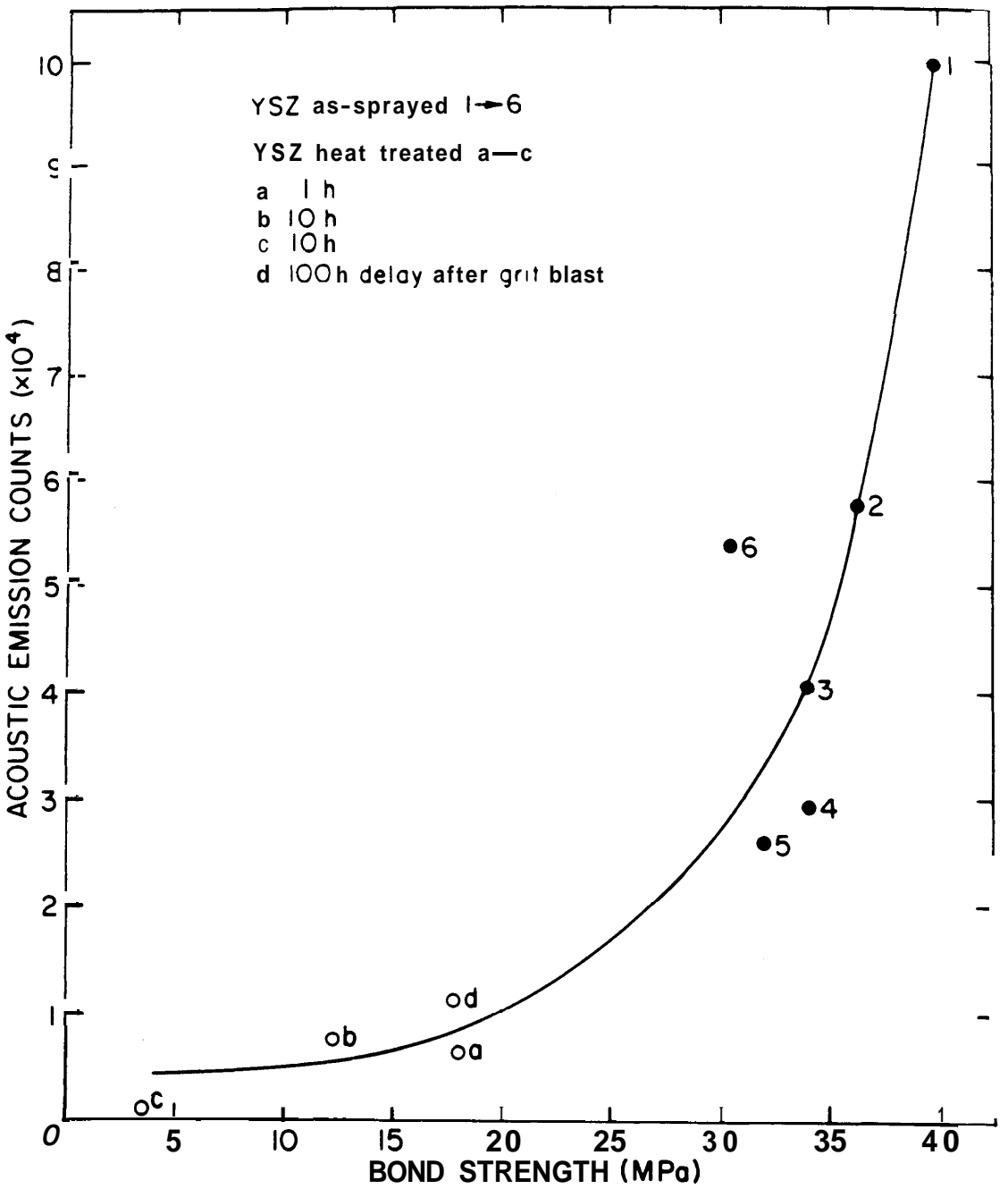


Fig. 7. Cumulative AE counts vs bond strength of the as-sprayed and treated YSZ plasma-sprayed coatings.

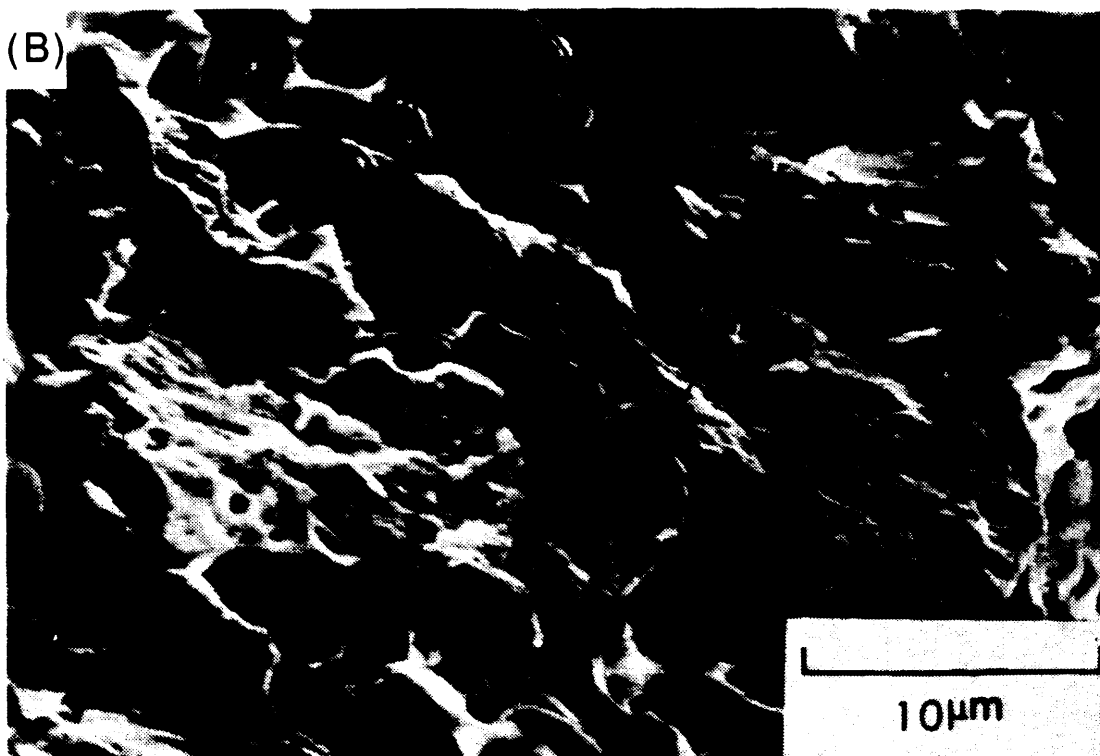


Fig. 8. Fracture surfaces of the failed YSZ coating: (A) adhesive-failure region showing interlamellar nature of the fracture; (B) cohesive-failure region showing both interlamellar (region "a") and translamellar fracture (region "b").

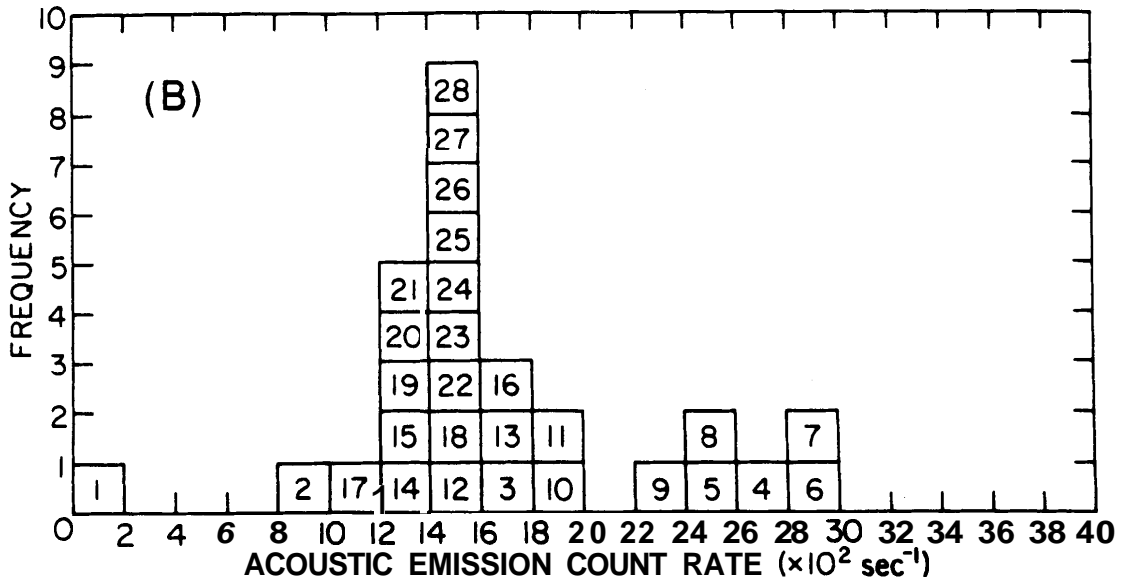
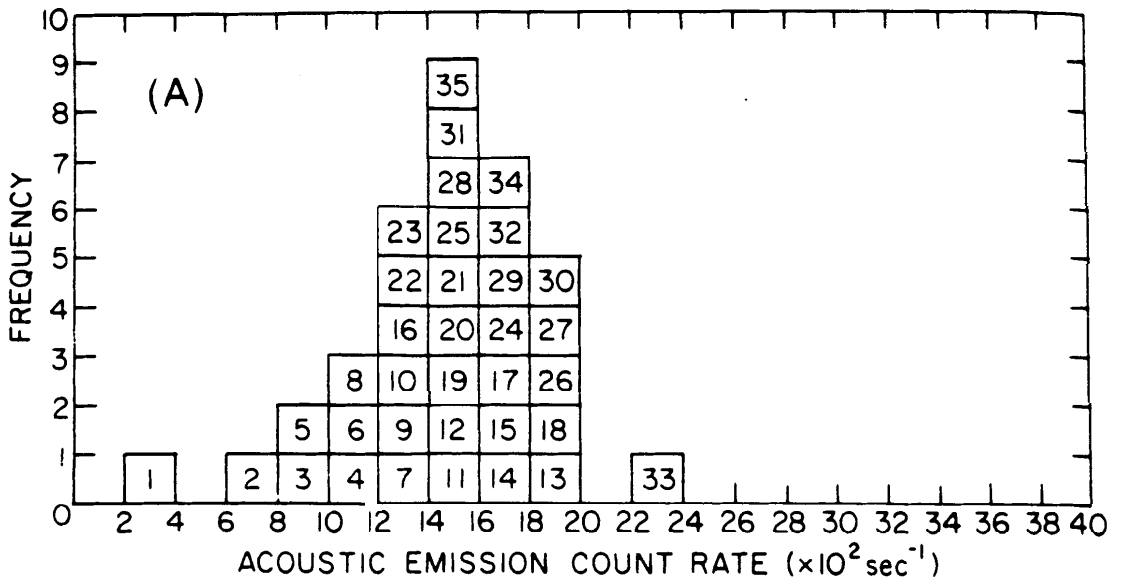


Fig. 9. The frequency of a specific count rate vs the count rate (where the numbers refer to the sequence in seconds) of a particular count rate: (A) the AE count rate increases with time, is maximum prior to failure, and corresponds to Fig. 5(A), i.e., skewed left; (B) the AE count rate increases to a maximum during the initial periods of the test and then decreases to a minimum prior to failure. This bimodal distribution corresponds to Fig. 5 (B), i.e., skewed right. (Counts at failure have not been included.)